The Backscattering Contribution of Soybean Pods at L-band

Yiwen Zhou*[a], Avinash Sharma[b], Mehmet Kurum[c], Roger Lang[a], Peggy O'Neill[d] and Michael Cosh[e]

[a] The George Washington University, Washington, DC, USA
[b] The Johns Hopkins Applied Physics Lab, Laurel, MD, USA
[c] Mississippi State University, Mississippi State, MS, USA
[d] NASA Goddard Space Flight Center, Greenbelt, MD, USA
[e] USDA-ARS Hydrology and Remote Sensing Laboratory, Beltsville, MD, USA

Abstract

L-band (1.25 GHz) radar measurements of a soybean canopy indicate that the emergence of seed pods is a significant contributor to the backscatter during the late stages of the growing season. In order to validate the measured data, a realistic scattering model of the soybean canopy is developed. The parameters of the soybean canopy and underlying soil used in the model vary over the growing season based on *in situ* measurements. Scattering amplitudes for soybean leaves are modeled analytically by using a thin disk approximation; stem and pods are jointly modeled using a numerical electromagnetic field solver. These scattering amplitudes are together incorporated into a coherent scattering model to obtain the backscattering coefficient for VV- and HH-polarizations. The modeling results show good agreement with the radar field measurements, having RMSEs of 0.51 dB for VV-pol and 1.1 dB for HH-pol. Both measured data and modeled results show that the change of soil moisture can be accurately monitored by L-band backscatter. It is also found that the difference between HH- and VV-polarized backscatter increases as the size of the soybean pods becomes larger. A method is developed here to estimate the number of pods in a soybean canopy based on polarimetric radar backscatter at L-band.

Keywords

Radar backscatter, Soybean growth and development, Soybean pods, ComRAD, Soil Moisture

1. Introduction

A model describing the microwave backscatter from a layer of vegetation is important for the study of active remote sensing of soil moisture and vegetation dynamics. The scattering amplitudes of the canopy scatterers are dependent on each plant and their density throughout the canopy (Steele-Dunne et al., 2017). To model an individual plant, the density, dielectric properties, size, and orientation of the major components of vegetation (e.g. stem, leaves, and fruit) need to be considered. The backscattering contributions of plant fruits, in particular, have important bearing on remote sensing of agricultural harvests. In the past, C-band or higher frequency radars have often been used to monitor agricultural crops due to their high sensitivity to vegetation constituents (Joerg et al., 2018). The penetration into the vegetation canopy of these high-frequency radars, however, is too weak to monitor the underlying soil moisture. The motivation of this paper is to explore the use of radar backscatter data at low microwave frequency (L-band) to monitor the growth of soybean pods, as well as the underlying soil conditions.

The reason for choosing L-band in this study is because radars operating at this frequency have been widely used by a number of Earth-observing satellites to sense the Earth's surface due to their strong penetration through clouds and vegetation canopies. The Advanced Land Observing Satellite (ALOS) was an Earth Observation satellite mission launched by the Japan Aerospace Exploration Agency in 2006 (Rosenqvist et al., 2007). It employed a Phased Array L-band Synthetic Aperture Radar (Palsar) to monitor the Earth's surface. Its operation stopped in

2011 and ALOS-2 (Kankaku et al., 2013) was launched in 2014 to continue Earth monitoring at L-band (1.2 GHz). Soil Moisture Active Passive (SMAP) is a NASA satellite launched in 2015 (Entekhabi et al., 2010). SMAP carries a combined radar and radiometer system for its primary mission of measuring soil moisture; its radar operates at 1.25 GHz and its radiometer operates at 1.4 GHz. The SMAP radar, however, stopped operating about 5 months after launch due to a power supply failure, although its radiometer continues to provide quality passive observations to the present time. The NASA-ISRO SAR (NISAR) is a new joint satellite mission developed by the USA and India whose main goal is to exploit synthetic aperture radar to map Earth's surface every 12 days (Rosen et al., 2015). It operates at the dual frequencies of L-band at 1.25 GHz and S-band at 3 GHz. The launch of NISAR is planned for 2022.

In order to assist the research of land remote sensing at L-band, the ComRAD (Combined Radar-Radiometer) truck-mounted microwave instrument system has been developed jointly by George Washington University and NASA Goddard Space Flight Center (O'Neill et al., 2006). ComRAD includes a quad-pol 1.25 GHz radar and a dual-pol 1.4 GHz radiometer sharing the same 1.22-m parabolic dish antenna. The resolution of ComRAD is about 4-5 m (depending on boom height and incidence angle), which is much higher than most of the satellite missions. Its main use is to obtain active/passive L-band data as a simulator of satellite sensors to refine the soil moisture retrieval algorithms for Earth-observing satellite missions.

In the past, there were very few research papers that describe the modeling of scattering from the fruits of agricultural crops at L-band. Monsivais-Huertero and Judge (2011) analyzed the backscatter from growing corn at L-band using the Michigan Microwave Canopy Scattering Model (MIMICS) (Ulaby et al., 1988) and the coherent model developed by Thirion et al. (2004). Their analysis indicated a possibility of monitoring the growth of corn at L-band. De Roo et al.

(2001) developed a semi-empirical backscattering model for a soybean canopy at L- and C- band with soil moisture inversion. Huang et al. (2015) developed a coherent scattering model for soybeans at L-band. In both De Roo and Huang models, however, the soybean pods were not taken into consideration.

Coherent scattering effects have been considered in this paper to model the scattering of a soybean canopy. Different from the energy-based radiative transfer method (Tsang, 1985), the coherent scattering model is based on electromagnetic waves in random media (Chauhan et al., 1991). The model consists of a layer of discrete random media over a dielectric half-space, with the mean field computed using the Foldy method (Foldy, 1945). The scatterers are then embedded in the mean medium and the Distorted Born Approximation (DBA) is employed to obtain the scattering coefficients for the canopy (Lang and Sidhu, 1983). Since the coherent method has shown significant improvements on matching radar data for a corn field (Lang et al., 2017; Sharma et al., 2020), it has been chosen to model the soybean canopy.

In this paper, the backscattering contribution of soybean pods at L-band is discussed based on modeled results and measured data taken by ComRAD over the reproductive stages of a soybean canopy prior to senescence. Ground truth data are used as parameters of the soybean scattering model to understand the relationship between the polarimetric L-Band radar backscatter and the dynamics in the soybean canopy and underlying soil moisture. Comparison between the modeled results and measured data provides a sound validation of the robustness of the model due to the large variation in soybean canopy parameters over the reproductive stages.

The paper is structured as follows: Section 2 introduces the *in situ* measurements taken from the soybean field. Measurements collected include the dimensions, biomass, and density of the plant constituents as well as the soil moisture and the surface roughness underlying the soybean canopy. In addition, backscatter observations from the soybean canopy by the ComRAD radar are presented in this section. In Section 3, a coherent model of the scattering of a soybean field is presented. For a single soybean plant, the leaves are represented by thin dielectric elliptical discs and their scattering amplitudes are computed via a thin disc approximation from Le Vine et al. (1985). The combined scattering amplitudes of soybean pods and a stem are found using a numerical EM solver. The scattering amplitudes of leaves, stems, and pods are then employed in the coherent discrete scatter model developed by Chauhan et al. (1991) to obtain backscatter from the soybean field over the reproductive stages. In Section 4, the backscattering coefficients from the soybean canopy - with and without the pods - are compared in order to demonstrate the contributions of soybean pods. The modeled results are also compared with the actual measurement results obtained by the ComRAD radar. The comparison is used to establish a relationship between the polarimetric radar backscatter and the counts of soybean seeds per square meter. Finally, the conclusion is presented in Section 5.

2. Soybean canopy measurements

2.1 Plant dimension and biomass measurements

The soybean fields used in this study were located at the Optimizing Production Inputs for Economic and Environmental Enhancement (OPE^3) site, which has been maintained and instrumented by the U.S. Department of Agriculture - Agricultural Research Service (USDA-ARS) located in Beltsville, MD. The soybeans were planted on June 14, 2012 and the *in situ* measurements were started on June 26, 2012, i.e. day of year (DOY) 178, and taken approximately once every week over the growing season. Plants were randomly selected from the measurement site for destructive sampling. The measured dimensions of leaf, stem, and pod are plotted in Fig. 1 for DOY 178-269 (Jun. 26 - Sep. 25). For each DOY in the figure, the points for plant height represent the average results of three different plants; the points for leaf represent the average results of fifteen leaves and the points for pod represent the average results of nine pods. In Fig.1, the point with error bar represents the mean ± standard error (SE). The standard error of the mean can be computed by:

$$SE_{i,j} = \frac{SD_{i,j}}{\sqrt{N_j}}, \tag{1}$$

where $SD_{i,j}$ is the standard deviation of the measurements of jth type of soybean constituents at ith day of experiment; N_j is the number of measurements made for jth type of constituents.

There are two main stages in the growth of a soybean plant: vegetative stage and reproductive stage, which correspond to the periods before and after the flowering of soybean plants, respectively. In Fig.1, DOY 178-198 is the period for the vegetative stage during which the leaves and stems develop. It is seen from the figure that the dimensions of leaf and stem increase rapidly until around DOY 200, when the reproductive stage starts.

The period from DOY 200 to DOY 269 is the reproductive stage of the soybean plants. The reproductive stage of soybeans can be further categorized into sub-stages of R1-R8 based on the growth of pods (Pederson, 2004). The period of each stage of a soybean's growth is dependent on the thermal time (T_t) with a unit of °C-day. The expression of thermal time is given as (Togliatti et al., 2019):

$$T_t(n) = \sum_{1}^{n} \left(\frac{T_{max}(n) + T_{min}(n)}{2} - T_{base} \right) \tag{2}$$

where n represents the number of days passed since planting; $T_{max}(n)$ and $T_{min}(n)$ are the maximum and minimum temperature for the n^{th} day after planting, respectively; T_{base} is the base temperature, below which the development of crop will no longer occur. Here, T_{base} is set to be 10° C (Togliatti et al., 2019; Abendroth, 2011). For the period of 2012 soybean measurements, the temperature data are obtained from an online source (https://www.timeanddate.com/weather/) and the thermal time is computed correspondingly. In Fig. 1, the thermal time, T_t, is given above the x-axis in red color. The information of thermal time can be used by future studies for comparing the growth of soybean plants in other locations and years that experience different weather conditions.

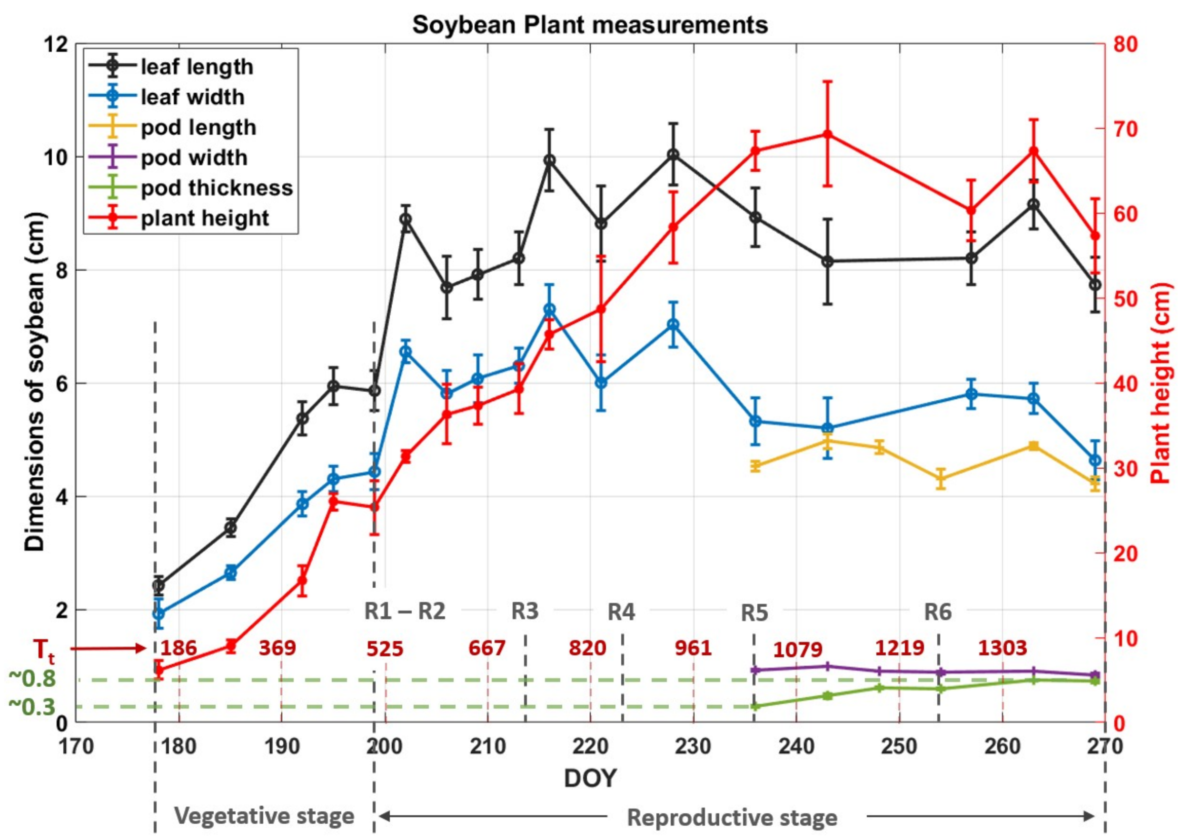

Fig. 1. Soybean plant dimensions as a function of DOY/Thermal time.

Based on thermal time, the approximate start dates of different R-stages are estimated and marked in Fig. 1. In the figure, DOY 213-269 covers from R3–R4 (beginning pod – full pod) to R5–R6 (beginning seed – full seed) and stops right before R7 (beginning of maturity). The recording of the pod dimensions started on DOY 236 where approximately the R5 (beginning seed) stage starts. It is seen that the dimensions of leaves and stems stay relatively consistent during the reproductive stage. Different from the other constituents, the pods become thicker during the reproductive stage as the seeds within the pods grow. The thickness of the pods changes approximately from 0.3 cm to 0.8 cm while the length and width of the pods remain almost constant as DOY goes from 236-269. The field measurement data for DOY 213-269 are documented in Table A.1 to provide a more detailed track of the growth of soybean plant constituents.

During the period of measurements, i.e. stages R3-R6, soybean pods are green. For stages R3-R4, a soybean pod is formed by a green shell with a thin layer of dry matter enclosed. The dry matter provides the nutrients for the development of beans (seeds). The forming of beans starts at stage R5. A soybean pod usually contains 2-4 beans covered with a green shell during stages R5-R6. Fig. 2 (Casteel, 2011) shows a closer look at soybean pods for stages R5 and R6. It is seen from Fig. 2 that the length and the width of pods stop growing while the thickness of the pods increases due to the forming of beans during stages R5-R6. The effects of the bean growth will be considered in the development of the soybean backscattering model in this paper.

The orientation of leaves is also recorded in the measurements and the leaf angle statistics for DOY 213-269 are plotted in Fig. 3. It is seen that the statistics of the leaf angle can be approximated by a $\cos\theta$ distribution function, with $0^\circ \leq \theta \leq 90^\circ$. Here, θ is the angle between the normal direction of the leaf surface and the normal direction of the ground. This information will be employed to model the backscatter of the soybean canopy in Section 3.

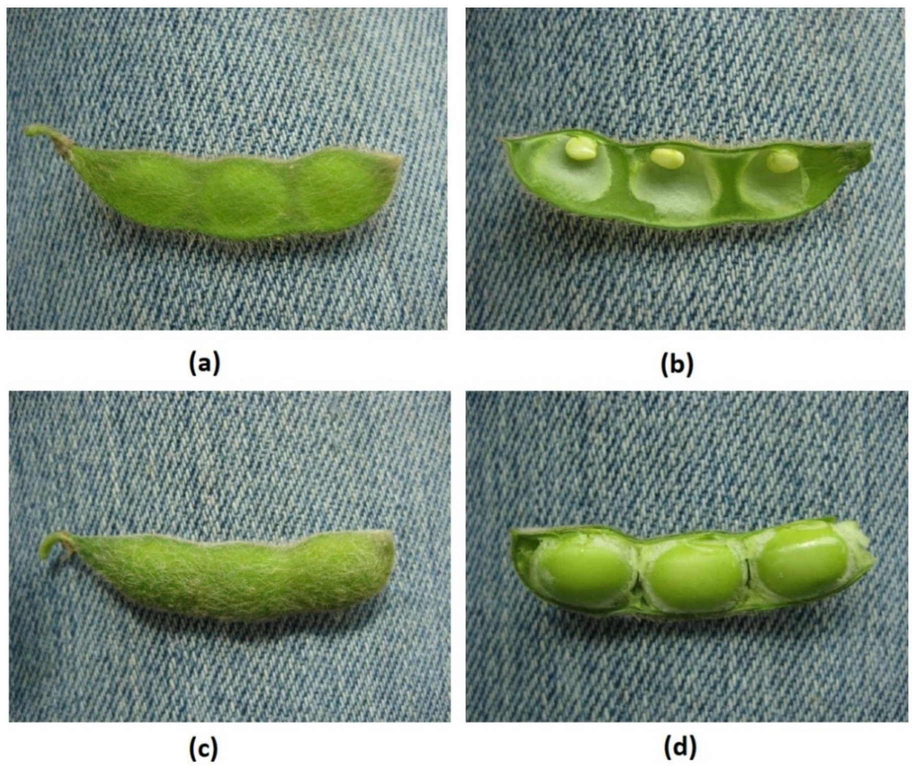

Fig. 2. Soybean pods - (a): soybean pod at the beginning of stage R5; (b): soybean pod of (a) with half the shell removed; (c): soybean pod at stage R6; (d): soybean pod of (c) with half the shell removed.

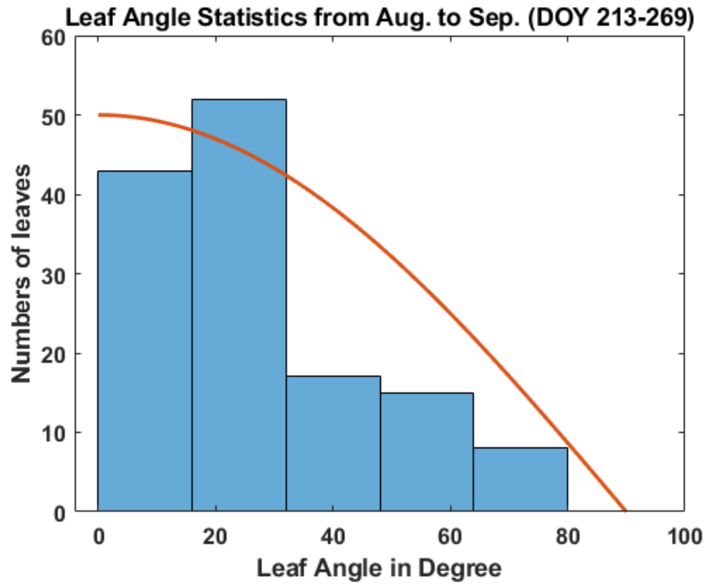

Fig. 3. Histogram of leaf orientation.

The gravimetric vegetation water content (GVWC) of the soybean plant constituents was also measured over the growing season. In this paper, GVWC is defined as the ratio of the difference between the fresh and dry mass of vegetation to the vegetation fresh mass (Wang et al., 2015). Three soybean plants were randomly picked on each sampling day and cut into stem, leaf and pod components. The petioles, which are the thin branches for supporting the leaves, are not considered since their effect on scattering is assumed to be small at L-band. The chosen components were sorted and placed into individual bags. The mass of the bags was recorded and then oven-dried for about 3 days at 70° C until the mass did not change. Finally, the mass of the bags was found again and the GVWC from the individual components was computed in percentage. The GVWC are plotted for stem, leaf, and pod through DOY 213-269 (stages R3-R6) in Fig. 4(a). It is seen that the GVWC of the soybean stem and pods decays slightly, while the GVWC of soybean leaves stay quite consistent during stages R3-R6. These results indicate that the dielectric constant of the soybean components remains approximately the same during this period.

The GVWC can then be converted to the wet biomass using the plant mass and density measurements. The wet biomass measurement results are plotted in Fig. 4(b) for stem, leaf, pod and whole plant. The red dashed line, which corresponds to the right y-axis, represents the percentage of the biomass of pods to the total biomass. Compared with other soybean constituents, pods have much greater contribution to the total biomass in the later stages. The rise of the pod biomass is mainly due to the increase of the pod size/thickness. Fig. 4(b) demonstrates that the soybean pods are the dominant contributor to the total biomass during reproductive stages and their scattering contributions need to be included in any accurate scattering model. The thermal time, T_t, is also given in Fig. 4(a) and (b) to provide a reference for future studies.

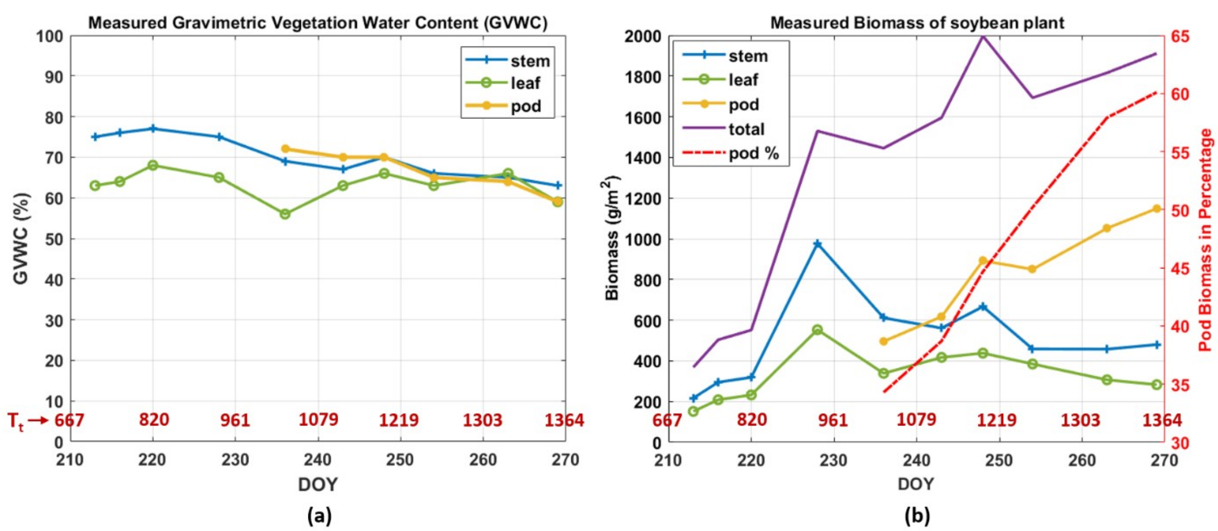

Fig. 4. (a): GVWC of soybean plant constituents; (b): Wet Biomass of soybean plant constituents.

2.2 Dielectric measurements

The dielectric constant of soybean pods was determined by a reflection technique. Since no dielectric measurements of soybean pods were performed in the summer of 2012, the measurements were made in 2019 for soybean plants in adjacent fields similar to those grown in

2012. The dielectric measurements were performed by an open coaxial probe which connected to a portable vector network analyzer (Keysight Fieldfox N9923A) to measure the reflection coefficient, Γ, from the surface of the soybean pods. The dielectric constant can then be determined by the formula from Stuchly, M and Stuchly, S (1980). Methanol was used as the calibration solution in the experiment since its dielectric constant is close to that of the soybean constituents; the dielectric constant of methanol is obtained from Gregory and Clarke (2012).

The dielectric measurements were made for soybean shells and beans separately by inserting the probe perpendicular to their cross-sections at various locations. Three different pods were used in each measurement and the average dielectric constants were recorded. The measurements were performed for two different fields during a three-week period (DOY 261–274/ Sep.18–Oct. 1). Three sets of the data were obtained from field #1 and one set of data was obtained from field #2. The soybean plants from field #1 were planted on Jun. 28 and the plants from field #2 were planted on May. 18. The results are shown in Table 1.

Based on the thermal time of planting, the pods from field #1 should have approximately reached stage R5-R6, which are comparable to the soybean measurements performed on DOY 242-256 in 2012. It is seen from the table that the dielectric constants of green pods stay relatively consistent during this period. The pods from field #2, which have already reached stage R7, have a much lower dielectric constant due to the loss of moisture. Since the stage R7 is later than the stages of soybeans in the 2012 measurements, the dielectric constants of soybean pods from field #2 are not considered in this study.

Days passed since planting	**Thermal Time (°C-day)**	**Soybean Field**	**Sample stage**	**Parts**	**Dielectric Constants**	
					Real	**Imag.**
82	1120	#1	R5	Beans	47	16
				Shells	46	8

89	1185	#1	R5	Beans	41	18
				Shells	37	15
95	1252	#1	R6	Beans	51	16
				Shells	49	9
130	1631	#2	R7	Beans	25	12
				Shells	22	8

Table 1 Soybean dielectric measurement data

In section 3, a pod will be modeled in one piece to avoid the complexity of modeling the shells and beans separately. Thus, the effective dielectric constant of the pods, ε_{eff}, is computed based on the percentage volume and the averaged dielectric constant of beans and shells. The dimensional measurements for a pod reaching R6 stage show that the beans and shells make up about 70% and 30% of the volume of an individual pod, respectively. Based on Table 1, the ε_{eff} of pods is estimated as 46-15j. These dielectric measurements and the previous GVWC results together indicate that the dielectric constant of soybean pods can be considered as a constant over the reproductive stages prior to R7.

Based on the measured data documented in Lang et al. (2004), the dielectric constants of soybean leaves and stems are set to be 23-9j and 15-5j, respectively. These dielectric constants are used in this paper for obtaining the analytic and the numerical solutions of soybean scattering. Note that the dielectric constants only have a small effect on the backscattering coefficients. For example, decreasing the dielectric constant of the pods by 20% only changes the backscattering coefficients by 0.4 dB.

2.3 Soil Type

Besides the soybean constituents, the underlying soil has a significant influence on radar backscatter. The test site has a soil texture that is characterized as a sandy loam, with 23.5% silt, 60.3% sand and 16.1% clay. The soil has a bulk density of 1.25 $g \cdot cm^{-3}$. To determine the soil moisture, several locations away from the radar footprint were sampled. A Delta-T theta probe was inserted into the surface and provided a measurement of the near-surface soil moisture. The probe is 6 cm in length, but the approximate depth contribution of L-band radiometry is generally taken to be about 0-5 cm. Therefore, the theta probe is calibrated to gravimetrically collect soil samples with a 0-5 cm depth. This method has been used throughout all of the soil moisture field experiments used for SMAP calibration/validation. The measured daily averaged volumetric soil moisture is documented in Table A.1 for DOY 213-269. Based on the soil type and moisture, the complex dielectric constant of the soil was computed using the Dobson model (Dobson et al., 1985, Peplinski et al., 1995a, 1995b).

The surface roughness of the soil was measured by a metal grid board. Numbers of points were chosen from two fields in the surface roughness measurements and the experiments were done along and across the soybean rows. The number of measurements and the measured results are given in Table 2. Due to the randomness of the measurements, the surface roughness was also calibrated by matching the radar backscatter data of the bare soil to the analytic rough surface model using the small perturbation method given by Fung and Chen (2009). The backscatter of the bare soil was measured for the soybean field after planting but before the emergence of soybean plants. The calibrated surface roughness has an RMS height of 0.7 cm and a correlation length of 12 cm, which has reasonable agreement with the measured data given in Table 2. Note that the largest change of surface roughness generally occurs during the first rain event since planting, which tends to smooth the surface. The surface roughness measurements in this study were made after the first rain event. The soil roughness was visually observed through the course of the experiment and it did not noticeably change. Therefore, surface roughness is treated as a constant in this study.

	# of Meas.	RMS height (cm)	Correlation Len. (cm)
Field #1 along	85	0.57	3.0
Field #2 along	110	0.56	20.2
Field #1 across	139	1.98	11.8
Field #2 across	77	1.84	13.2

Table 2 Surface roughness measurement results

2.4 ComRAD Radar measurements

The Combined Radar/ Radiometer (ComRAD) truck-mounted microwave instrument (O'Neill et al., 2006) is a combined system operating as a radar at 1.25 GHz and as a radiometer at 1.413 GHz. It is mounted on a 19-m hydraulic boom truck as seen in Fig. 5. The radar and radiometer share a parabolic dish antenna with a Cassegrain-like feed. The feed is implemented with a circular waveguide having two orthogonally placed wire probes, one to support horizontal polarization (HH-pol) and the other to support vertical polarization (VV-pol). The cross-pol data are not considered in this study due to the difficulties in the calibration of cross-pol channels compared to co-pol channels. For this study, the radar has a fixed incident (elevation) angle of 40° to the soybean field. The radar acquires data by sweeping in a 120° azimuth range with a 2° increment; the sweeps are repeated every few hours throughout the day. The daily averaged backscattering coefficients are plotted in Fig. 6 with error bars. Similar to Fig. 1, the error bars represent the standard error of the mean. The measured volumetric soil moisture (VSM) results are also plotted in Fig. 6 to compare with the backscattering coefficients from the radar.

Fig. 5. ComRAD system mounted on a 19-m boom truck.

It is seen from Fig. 6 that most of the soil moisture peaks are well captured by the radar backscattering data. Note that there are no data between DOY 230-234 and DOY 244-257 due to radar maintenance. The correlation between radar backscatter and VSM is evaluated by the correlation coefficient (R); the results of R are provided in Table 3 for HH- and VV-pol. To further investigate the variation of the radar data corresponding to the change in VSM, temporal series of the difference in radar backscatter (dB) on two consecutive measurements, i.e. $\sigma^0(n+1) - \sigma^0(n)$, and the ratio of VSM on the corresponding dates, i.e. VSM(n+1)/VSM(n), are generated (Balenzano et al., 2011). Here, n is the sequential number of the measured data. The correlation coefficient between these two temporal series is computed and denoted as R_Δ, which has been given for HH- and VV-pol in Table 3. It is seen that the R coefficient for VV-pol is slightly greater than the R of HH-pol. This difference might be due to the effect of the soybean canopy, which will be discussed in the next paragraph. The coefficient R_Δ shows that the changes in both HH- and VV-pol backscatter are strongly correlated to the changes in VSM over the reproductive stage.

Backscatter vs. VSM	R	R_{Δ}
HH-pol	0.52	0.89
VV-pol	0.78	0.81

Table 3 correlation coefficient between Radar Backscatter and VSM

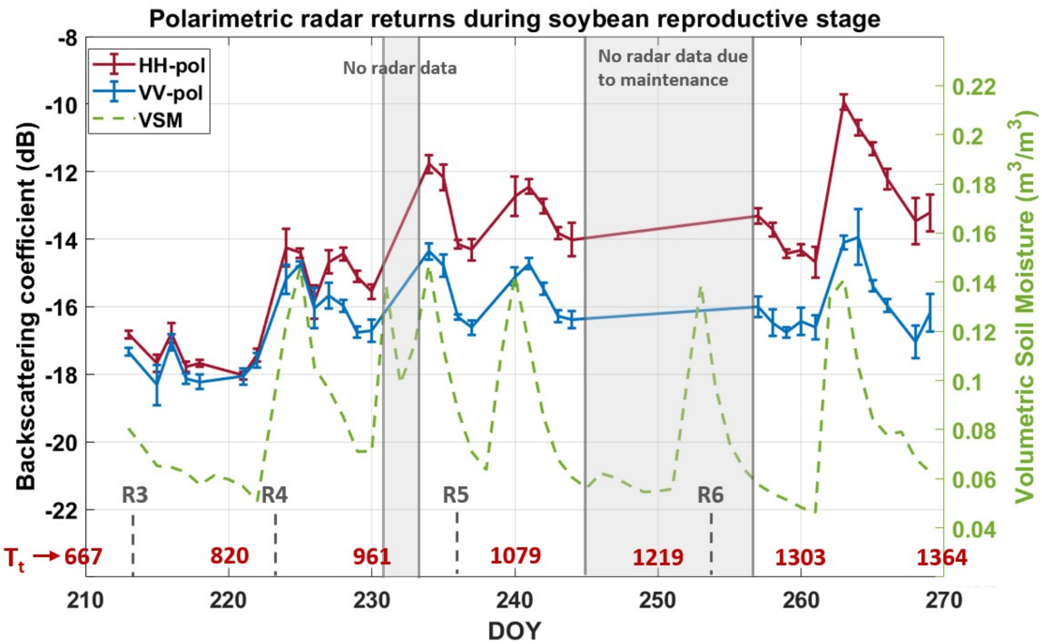

Fig. 6. Polarimetric radar backscattering data vs. volumetric soil moisture.

To better understand the relationship between backscatter and vegetation dynamics, the reproductive stages are also marked in this figure. From R3-R4 stages (beginning - full pod), the radar backscatter for HH-pol and VV-pol are about the same. As the pods reached the full stage (around DOY 223), the beans inside the pods started to form and the pods became thicker. It can be seen from Fig. 6 that the HH-pol and VV-pol begin to diverge after stage R4 and onwards, with HH-pol being higher while VV-pol remaining about the same level. The later the reproductive stage is, the bigger the difference between HH-pol and VV-pol that can be observed. The increase in HH-pol due to the growing of pods could be the reason why the correlation between HH-pol and VSM is slightly weaker than the correlation between VV-pol and VSM.

This phenomenon indicates that the growth of beans can be observed by the radar at L-Band frequencies. It motivates the study of soybean pod modeling in this paper. In the next section, a combined numerical and analytic model will be proposed to analyze the difference between the backscatter for HH and VV polarization.

3. Soybean canopy backscattering model

3.1 Soybean Canopy Coherent Backscattering Model

The soybean canopy is modeled as a single layer of discrete random scatterers over a dielectric half-space that has a rough underlying surface. The random layer consists of three types of scatterers: leaf, stem and pod. The pod and stem will be modeled together in FEKO (commercially available software package) as one type of scatterer. The other type of scatterer is soybean leaves, which are modeled analytically. Fig. 7 shows the medium layer with two individual components highlighted to represent the two types of scatterers. These two types of scatterers are assumed to be statistically independent in zenith and azimuth direction. Note that the soybean petioles have not been taken into account since they are too small to have a significant contribution to the total backscatter at L-band. Numerical results show that their backscatter is about 15-25 dB less than the total backscatter of soybean plants.

There are three dominant types of backscatter: direct (or volume) backscatter, direct-reflected (or double-bounce) backscatter, and surface backscatter. The total backscatter is approximately the sum of all of the three backscattering terms, which can be written as,

$$\sigma^0_{qq} = \sigma^0_{d_{qq}} + \sigma^0_{dr_{qq}} + \sigma^0_{s_{qq}} \quad (3)$$

where subscript $q \in (h, v)$ is the polarization type, $\sigma^0_{d_{qq}}$ is the direct backscattering coefficient; $\sigma^0_{dr_{qq}}$ is the coherent direct-reflected backscattering coefficient, and $\sigma^0_{s_{qq}}$ is the surface backscattering coefficient with attenuation from the soybean canopy. Note that only the like-pol is considered in this analysis.

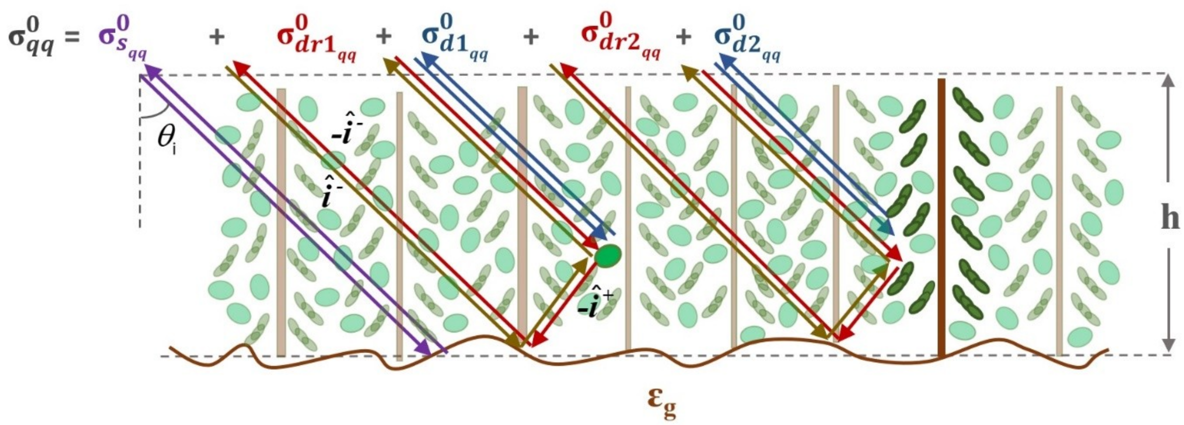

Fig. 7. Ray trajectories for the soybean canopy scattering model.

These three types of scattering are also depicted in Fig. 7. In the figure, $\sigma^0_{d1_{qq}}, \sigma^0_{dr1_{qq}}$ and $\sigma^0_{d2_{qq}}, \sigma^0_{dr2_{qq}}$ represent the direct and direct-reflected backscatter for the leaves and pods-stem, respectively. Here subscript 1 refers to leaves and subscript 2 refers to stems/pods. Since scatterers of type 1 and 2 are independent of each other, eq. (3) can be written as:

$$\sigma^0_{qq} = \sigma^0_{d1_{qq}} + \sigma^0_{dr1_{qq}} + \sigma^0_{d2_{qq}} + \sigma^0_{dr2_{qq}} + \sigma^0_{s_{qq}} \tag{4}$$

It can be seen from the figure that $\sigma^0_{dr1_{qq}}$ and $\sigma^0_{dr2_{qq}}$ are the combined backscatters from the fields with two different paths (see red and brown arrow-lines in Fig. 7). Coherent terms have been taken into account for computing the direct-reflected backscatter; the equations to compute the total backscatter are documented in Chauhan et al. (1991). Note that a time variation of exp(jωt) is assumed and suppressed in this paper. In this section, the equations for computing the soybean backscattering terms are reproduced below:

$$\sigma^0_{dl_{jqq}} = 4\pi\rho_j \left\langle \left| f_{jqq}\left(-\hat{i}^-, \hat{i}^-\right) \right|^2 \right\rangle \left[\frac{1 - e^{-4\,\mathrm{Im}\,\kappa_q h}}{4\,\mathrm{Im}\,\kappa_q} \right]; \quad \sigma^0_{drj_{qq}} = 16\pi\rho_j R_{sq} \left\langle \left| f_{jqq}\left(-\hat{i}^+, \hat{i}^-\right) \right|^2 \right\rangle \cdot h \quad \text{for } j=1,2 \qquad (5)$$

where ρ_j is the volume density of j[th]-scatterer type; h is the canopy height; $f_{jqq}\left(-\hat{i}^-, \hat{i}^-\right)$ and $f_{jqq}\left(-\hat{i}^+, \hat{i}^-\right)$ are the backscattering and bistatic scattering amplitudes of the j[th]-scatterer type, respectively. Here, $\hat{i}^-$ is the direction of the incident wave with an angle of θ_i; $\hat{i}^+$ is the direction of the reflected wave. In eq. (5), κ_q is the propagation constant through the canopy; it can be written as $\kappa_q = k_0 \cos(\theta_i) + \delta\kappa_q$ where k_0 is the free space propagation constant, with $\delta\kappa_q$ given in Chauhan et al. (1991):

$$\delta\kappa_q = \sum_{j=1}^{2} \frac{2\pi\rho_j}{k_0 \cos(\theta_i)} \left\langle f_{jqq}\left(\hat{i}^-, \hat{i}^-\right) \right\rangle . \qquad (6)$$

Here, $\left\langle f_{jqq}\left(\hat{i}^-, \hat{i}^-\right) \right\rangle$ is the forward scattering amplitude.

The factor R_{sq} appearing in eq. (5) is the reflectivity at the surface of the canopy. R_{sq} can be expressed as the reflectivity of the ground, R_{gq}, times the two-way attenuation factor within the canopy as follows:

$$R_{sq} = R_{gq} e^{-2\alpha_q h}, \qquad (7a)$$

where $\alpha_q = 2\,\mathrm{Im}(\delta\kappa_q)$ is the attenuation constant in the canopy. The reflectivity of the ground can be decomposed into a product of the rough surface factor times the reflectivity of the flat ground surface:

$$R_{gq} = \exp\left[-\left(2k_0\sigma_h\cos\theta_i\right)^2\right] R_{gq}^0, \tag{7b}$$

where σ_h is the RMS height of the rough surface and $R_{gq}^0 = \left|\Gamma_{gq}\right|^2$. Here, Γ_{gq} is the Fresnel reflection coefficient for $q \in (h, v)$ polarization.

In eq. (5) and (6), $\langle\ \rangle$ is the sign for average. It indicates that the scattering amplitudes are averaged over the orientation angles, θ (zenith angle) and ϕ (azimuth angle) with a probability density $p(\theta, \phi)$. Here, θ and ϕ are assumed to be independent random variables. As a result, $p(\theta, \phi)$ can be written as $p(\theta, \phi) = p(\theta)p(\phi)$. For leaf, $\left\langle f_{l_{qq}}\left(-\hat{i}^-, \hat{i}^-\right)\right\rangle$ can be expressed as:

$$\left\langle f_{l_{qq}}\left(-\hat{i}^-, \hat{i}^-\right)\right\rangle = \int_{\theta=0}^{\pi/2}\int_{\phi=0}^{2\pi} f_{l_{qq}}\left(-\hat{i}^-, \hat{i}^-, \theta, \phi\right) p(\theta) p(\phi)\, d\theta\, d\phi. \tag{8}$$

In this study, $\left\langle f_{l_{qq}}(\cdot)\right\rangle$ is the average scattering amplitude of a single leaf, which can be solved analytically via a thin disc approximation from Le Vine et al. (1985). In the analytical model, the leaves are assumed to have a uniform distribution in azimuth direction, i.e. $p(\phi) = \frac{1}{2\pi}, 0 < \phi < 2\pi$. For the zenith direction, the distribution follows the statistics given in

Fig. 3, which has an approximate cosine distribution, i.e. $p(\theta) = \cos\theta, 0 < \theta < \pi/2$. The other scattering amplitude, $\left\langle f_{2_{pq}}(\square) \right\rangle$, is the average of the numerical solution of the pods-stem model. The procedure for averaging $f_{2_{pq}}$ will be discussed in section 3.2.

The surface backscattering coefficient is computed by using the Small Perturbation Method introduced by Fung and Chen (2009). The $\sigma^0_{s_{pq}}$ in eq. (4) can be obtained by multiplying the surface backscattering coefficient with the attenuation factor from the soybean canopy. Finally, by substituting $\sigma^0_{s_{pq}}$, $\sigma^0_{d1_{pq}}, \sigma^0_{dr1_{pq}}$ and $\sigma^0_{d2_{pq}}, \sigma^0_{dr2_{pq}}$ into eq. (4), the backscattering coefficient for the soybean canopy can be computed.

3.2 Numerical modeling of the scattering of stems and pods for a soybean plant

In the past, a dielectric cylinder model (Seker and Schneider, 1988) was used to model the fruits of agricultural crops in order to find their scattering amplitudes. The analytic method, however, is not accurate enough for the case of soybean pods since their cross-section is not a typical cylinder. In addition, since soybean pods are usually clustered, another advantage of using the numerical model is that the total contributions from the pod clusters can be determined from the model. The clusters act as bigger scatterers which can significantly enhance the contribution of pods in scattering. In this paper, a numerical model built in FEKO is proposed for solving for the scattering amplitude of soybean pods.

As previously mentioned, a soybean pod is formed by a green shell with 2-4 ellipsoid beans aligned inside. In the numerical model, a single pod is assumed to have three beans, which is the most common case in nature. The three beans are modeled by three adjacent ellipsoids. Based on the measured thickness of the soybean shells, the short and long radii of these adjacent ellipsoids are then expanded by 1.5 mm to account for the layer of shell in the model. Note that since there is not a big difference between the dielectric constant of the shell and the beans (see Table 1), it is not necessary to define different dielectric objects in FEKO to distinguish the shell and beans. This assumption also simplifies the model and reduces the time required for the simulation. In the model, each one of the ellipsoids has a slightly different orientation angle (see Fig. 2). In the 2012 field measurements, the number of beans of an individual soybean plant was only recorded for DOY 236, 248 and 263 (Aug. 23rd, Sep. 4th and Sep. 19th). The average number of beans per plant from the measurements is 94. In this study, the number of pods per plant is set to be 32, or equivalently, 96 beans. This assumption also agrees with the normal range of 26-38 pods recorded in Casteel (2011). The soybean pods are modeled together with a vertical stem. The stem has an approximate dielectric constant of 15-5j (Lang et al., 2004) and the averaged radius and height of the stems is 3.5 mm and 43 cm, respectively; these dimensions do not vary much over the reproductive stages. The leaves are not considered in the numerical model since they are so thin (0.2 mm to 0.3 mm) compared with wavelength that the interaction between leaves and other scatterers is very small. The analytic method is quite accurate for finding the scattering amplitude of leaves.

Most of the soybean pods emerge on or near the stems of plants, a condition which has been assumed for constructing the numerical model in FEKO. The variations in the vertical orientations of the pods are simulated by assigning different orientation angles to the ellipsoids that are used to form the pod. These orientation angles are represented by θ_1, θ_2 and θ_3 for the three ellipsoids from top to bottom; see Fig. 8(a). There are three different combinations for the orientation angles of pods defined in the numerical model --- type I: θ_1=5°, θ_2=10°, θ_3=15°; type II: θ_1=10°, θ_2=20°, θ_3=30° and type III: θ_1=20°, θ_2=30°, θ_3=40°. For a soybean plant, the number of the three different types of pods are in a ratio of 1:2:1 since most of the pods have orientations that are close to type II in nature.

The numerical model also considers the growth of the beans by varying their dimensions within the pod over the bean growing season. The growth of beans is categorized in three different stages: beginning seed or full-pod (R4), medium-seed (R5-R6), and full-seed (R6). As mentioned previously, the growing of beans only increases the thickness of the pods while the length and the width of pods do not change significantly. Based on this fact, the dimensions (length×width×thickness) of the pods are set to be 4.6 cm×0.9 cm×0.3 cm, 4.6 cm×0.9 cm×0.6 cm and 4.6 cm×0.9 cm×0.9 cm for the stages of beginning-seed, medium-seed and full-seed, respectively. The numerical models for a soybean plant at beginning-seed and full-seed stage are shown in Fig. 8(b) and (c), respectively.

In the numerical model, electromagnetic waves are incident at a 40° angle; this is the same incident angle used by the ComRAD system. H and V polarized waves are analyzed separately to obtain the backscattering amplitudes of the pods and the stem.

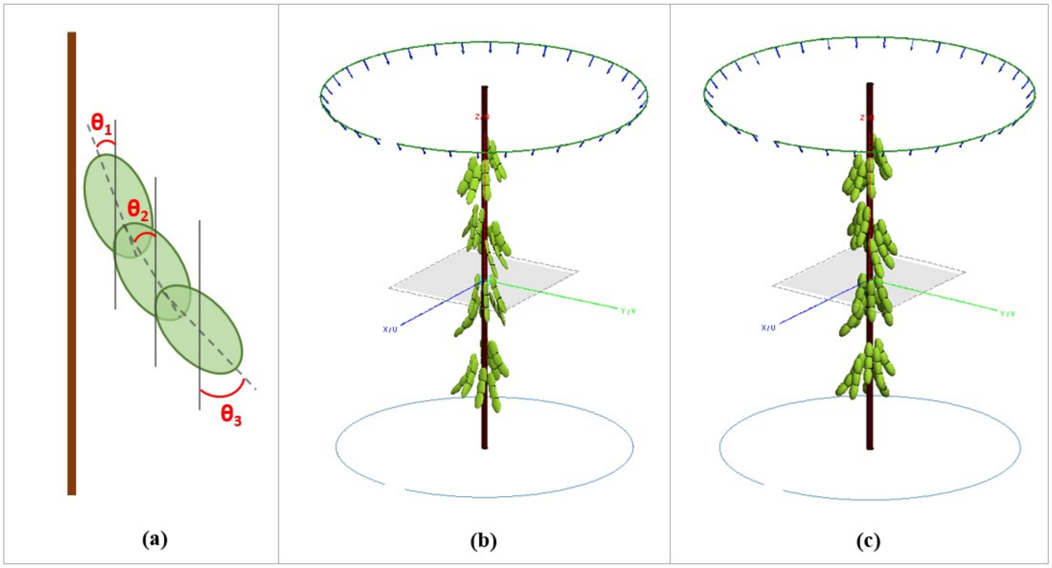

Fig. 8. Scattering model of soybean pods and stems in FEKO - (a): structure of soybean pod model; (b): multiple pod and stem model at beginning-seed stage; (c): multiple pod and stem model at full-seed stage.

As mentioned previously, the model is a compound of a single vertical stem and clusters of pods. The clustered pods are placed near the stem at selected heights and selected azimuth orientations (based on visual evidence) to represent a typical structure found in a soybean plant. It is assumed that the pod-stem scatterer is uniformly distributed in the azimuth coordinates.

Thus, the averaging of the scattering amplitude, $\left\langle f_{2}(\ ) \right\rangle$, can be done by a uniform azimuthal rotation of the structure.

When using the numerical model, it is more convenient to rotate the incident waves rather than rotate the model; this technique simplifies the processing of the EM solver. In performing the azimuthal average, the incident waves are distributed uniformly in a step size of 10°. These incident waves are shown by the blue arrows above the plant models in Fig. 8 (b) and (c).

At each individual incident angle, the back, forward and bistatic scattering amplitudes are computed (see Fig. 7). Averaging is then performed based on the scattering amplitudes from all incident waves for each model (beginning-seed model, medium-seed model, and full-seed model). This numerical solution of pod-stem compound and the analytic solution of leaves are integrated into the coherent canopy backscattering model to obtain the backscattering coefficient of the soybean canopy.

4. Comparison between the modeled results and measured data

4.1 Analysis of the modeled results

In this section, a comparison between the measured data and modeled results is presented. This analysis focuses on the reproductive stage of soybean plants from Aug.11th, 2012 to Sep. 25th, 2012 (DOY 224-269) since the pod data are documented for this period. A program is used to calculate the scattering amplitude of a single soybean leaf analytically. The density and dimensional parameters of soybean leaves used in the program are based on a least-squares fit to the measurement data given in Table A.1 for DOY 224-269. The fitted results are plotted in Fig. 9. As introduced in section 3.2, the scattering amplitudes of the pods-stem scatterer for three different reproductive stages are obtained by FEKO. Finally, the total coherent backscattering coefficient from the soybean canopy is computed using eq. (3). Table 4 summarizes the parameters that are used in the numerical and analytic model. Most of the parameters in the table have already been explained in the previous sections.

Based on the numerical results and parameters given in Table 4, the total backscattering coefficient is computed for HH-pol and VV-pol on each individual DOY. The pod size in the numerical model changes as DOY increases. The stages of beginning-, medium-, and full-seed correspond to DOY 224-230, DOY 234-244 and DOY 257-269, respectively.

Incident Angle		40°
Frequency		1.25 GHz
Stem and pods for a single plant (numerical model by FEKO)	Stem dimensions (cm): radius × length	Average of measured data given in Table A.1: 0.35×43

	Dielectric constant of stems	Obtained from literature: 15-5j
	Number of stems per plant	1
	Pod dimensions (cm): length × width × thickness	Average of the measured data given in Table A.1: -Beginning seed:4.6×0.9×0.3 -Medium seed: 4.6×0.9×0.6 -Full seed: 4.6×0.9×0.8
	dielectric constant of pods	measured in the lab: 46-15j
	number of pods per plant	32
Single leaf (analytic model in Fortran)	Leaf major and minor radius, Leaf thickness	Fitted values based on measurement data in Table A.1
	Dielectric constant of leaf	Obtained from literature: 23-9j
Macro parameters (canopy scatter model in Fortran)	Canopy height	Fitted values based on measurement data given in Table A.1
	Density of leaves (#/m^2)	Fitted values based on measurement data given in Table A.1
	PDF of leaves	$\cos(\theta)$, $0^\circ \le \theta \le 90^\circ$
	Density of soybean plants (#/m^2)	13
	Volume soil moisture	*In situ* measured data

Table 4 Summary of the input parameters to the canopy scatter model

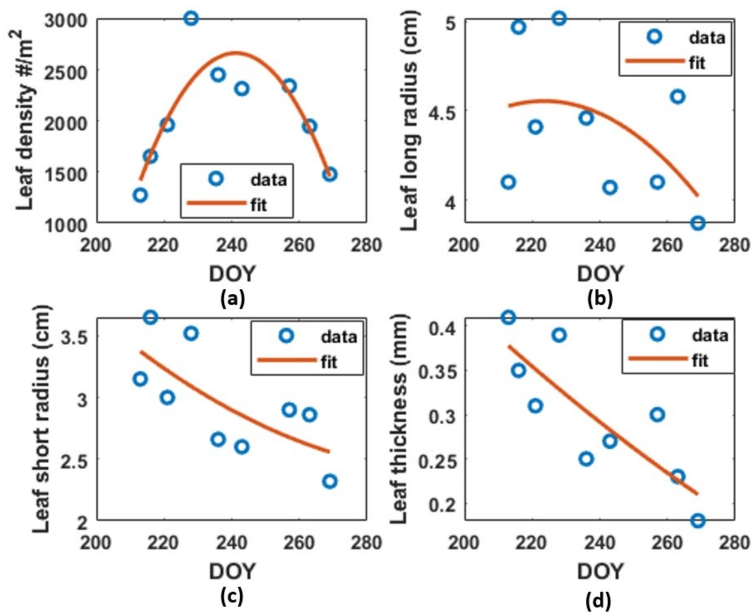

Fig. 9. Leaf parameters fitting - (a): Leaf density (#/m^2); (b): Leaf long radius (cm); (c): Leaf short radius (cm); (d): Leaf thickness (mm).

Besides the model for the soybean plant with pods, the backscattering coefficient of a soybean plant without pods is also computed. In the rest of this paper, the models with and without pods will be denoted as soybean-pod model and no-pod model for convenience. The no-pod model is an analytic model that only takes the leaves and stems into account. The scattering of leaves is computed analytically using the same method as mentioned before. The stem is treated as a thin cylinder and its scattering amplitude is found by using the formula in Chauhan et al. (1994). All the other parameters remain the same in this model except for the non-existence of pods.

Comparisons between the modeling results and the radar backscattering data are plotted in Fig. 10 as a function of DOY as well as thermal time, T_t. In general, the soybean-pod model has higher backscattering for both HH and VV polarizations compared with the no-pod model. The soybean-pod model has much better agreement with both HH- and VV-pol measurements, while the no-pod model underestimates the backscatter, especially during full-seed stage.

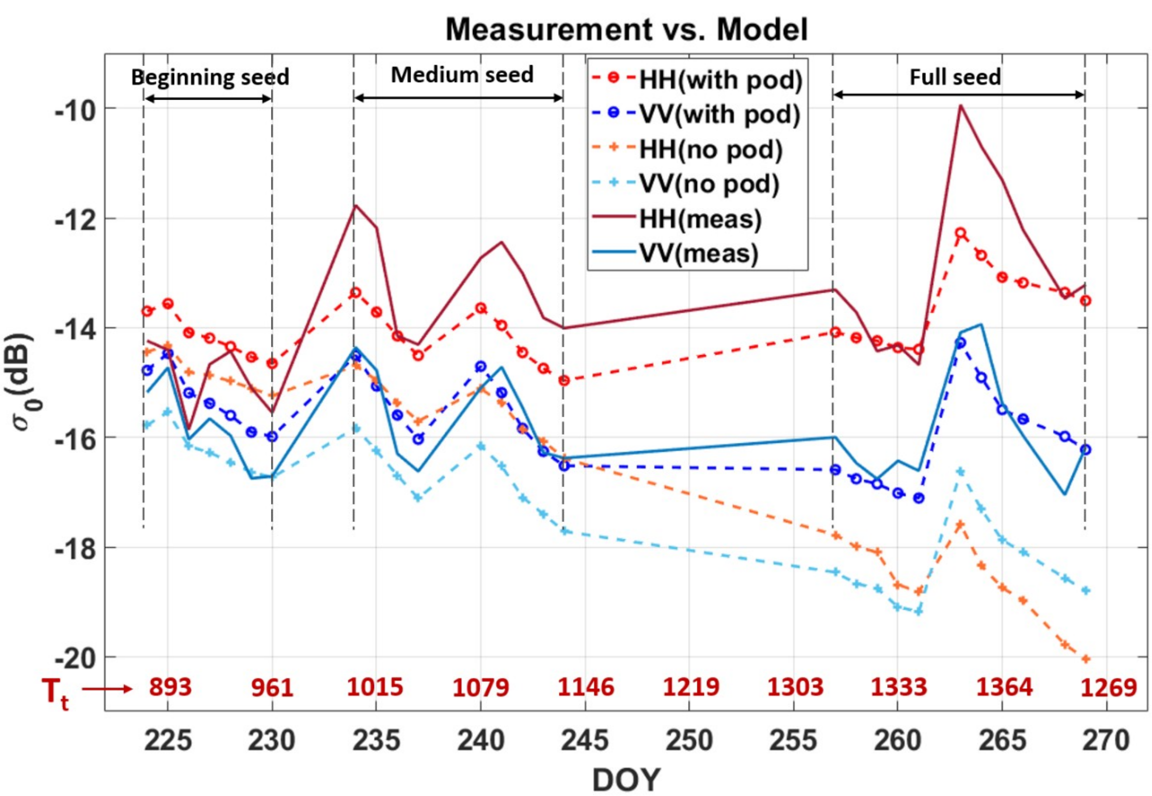

Fig. 10. Measured data vs. modeling results

At the beginning-seed stage, the soybean-pod model slightly overestimates the backscatter for HH and VV pol while the no-pod model has a good match to the data. During this period, the leaf is the dominant contributor to the backscatter; thus, both the soybean-pod and no-pod model strongly depend on the leaf size and density. During the medium-seed stage, the scattering from the pods becomes greater as the pods get thicker. The soybean-pod model hence predicts higher HH- and VV-pol backscattering compared with the no-pod model. The increase in total backscatter due to pod backscattering leads to better agreement between the soybean-pod model and the measurement data. At the full-seed stage, the soybean-pod model, which successfully predicts the slight increase of VV-pol and the large enhancement of HH-pol backscatter, has a much better match to the measurement data compared with no-pod model. The no-pod model predicts even lower HH-pol due to the loss of leaves and the shrinkage of leaf size. It can also be seen from both the measured and the modeled results that the difference between the HH-pol and VV-pol is strongly dependent on the size of the soybean pods. Hereinafter, the difference in backscatter between HH-pol and VV- pol is denoted as $\Delta\sigma^0_{HH\text{-}VV}$.

The peaks in the soybean-pod and no-pod model correspond to rain events as would be expected. However, most of the peak values for HH-pol predicted by the models are underestimated when compared to the data. This underestimation may be due to the presence of dew or rain drops on the surface of soybean plants that increases the effective dielectric constant of plant scatterers. This effect, however, is not considered in the modeling of soybean plants.

To quantitatively evaluate the performance of the soybean-pod and no-pod models, the root mean square error (RMSE) between the modeling results and measurements is computed by:

$$\mathrm{RMSE} = \sqrt{\frac{1}{N}\sum_{i=1}^{N}\left[\sigma^0_{meas}(i) - \sigma^0_{model}(i)\right]^2} \tag{9}$$

where N is the total number of samples shown in Fig. 10, $\sigma^0_{meas}(i)$ and $\sigma^0_{model}(i)$ are the measured and modeled backscattering coefficients for i^{th} day of experiment, respectively. The RMSE is computed based on results in dB and given in Table 5. It is clearly seen that the soybean-pod model has better agreement with the measured data for both VV and HH polarization than the no-pod model. For both the soybean-pod and no-pod models, VV-pol has better agreement with the measured data.

Model / Polarization	RMSE (dB)		R Coefficient	
	With pods	No pods	With pods	No pods
VV	0.51	1.8	0.78	0.56
HH	1.1	4.1	0.52	-0.31

Table 5 RMSE and R coefficient between modeling results and measured data

To further understand the correlation between the measurements and the model, the correlation coefficient (R) between σ^0_{meas} and σ^0_{model} is reported in Table 5 and σ^0_{model} is plotted against σ^0_{meas} in Figure 11. As expected, Table 5 shows that the soybean-pod model has a stronger correlation with the measured data compared to the no-pod model. Therefore, the scattered points of the soybean-pod model, as shown in Fig. 11, are closer to the linear-least-squares line than the no-pod model. Note that the correlation coefficient for the no-pod model is a negative value, which indicates that the behavior of the no-pod model is opposite to that of the measured data. This behavior can also be observed from Fig. 11(a). In summary, both the RMSE and R coefficient clearly demonstrate that the accuracy of the soybean scattering model is significantly improved by including the contribution of pods.

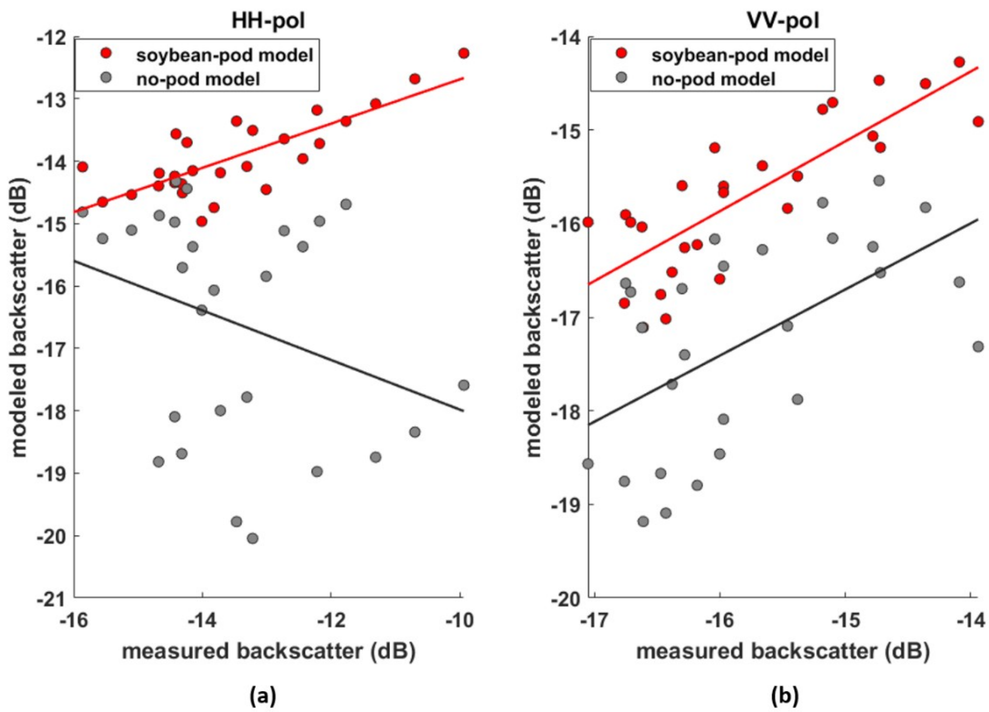

Fig. 11. Scatter plot of measured data against modeled results, where the line represents the least square fit of the scattered points. (a): is for HH-pol and (b): is for VV-pol.

4.2 Analysis of the difference between HH-pol and VV-pol backscatter

As previously mentioned, the difference in backscatter between HH- and VV-pol, $\Delta\sigma^0_{HH\text{-}VV}$, indicates the growing of the pods. To understand this phenomenon, the values of $\Delta\sigma^0_{HH\text{-}VV}$ are computed by converting the scattering coefficients σ^0_{HH} and σ^0_{VV} into their linear values and subtracting σ^0_{VV} from σ^0_{HH}. The difference $\Delta\sigma^0_{HH\text{-}VV}$ is then converted back to dB and plotted in Fig. 12 (a) for the soybean-pod model, no-pod model, and the measured data as a function of DOY. The growth stages of the pods are also given in the figure. As expected, the $\Delta\sigma^0_{HH\text{-}VV}$ for the no-pod model has a poorer performance than the performance of the soybean-pod model, in particular for the full-seed stage. Note that the curve for the no-pod model stops at

DOY 261 due to the fact that σ^0_{VV} is greater than σ^0_{HH} after DOY 261. For the soybean-pod model, $\Delta\sigma^0_{HH-VV}$ is not linearly related to the pod size. The modeled $\Delta\sigma^0_{HH-VV}$ increases slightly from beginning-seed to medium-seed stage, while it has a big enhancement from the medium-seed to full-seed stage. Considering all of the reproductive stages, the modeled $\Delta\sigma^0_{HH-VV}$ is closest to the measured $\Delta\sigma^0_{HH-VV}$ when the pods reach full-seed stage. This is the time when the beans are large enough to be detected by the L-band radar. As a result, it is more accurate to use the polarimetric L-band radar data to predict the soybean yield at the full-seed stage. Compared with the measured data, the soybean-pod model underestimates $\Delta\sigma^0_{HH-VV}$ for rainy days. Again, this might be due to the fact that the model hasn't taken the presence of water on the surface of plant into account.

An investigation has also been made into the relationship between the number of pods and $\Delta\sigma^0_{HH-VV}$. Based on the analytic model, $\Delta\sigma^0_{HH-VV}$ is computed for three cases: 24 pods per plant, 32 pods per plant and 40 pods per plant. The test is based on the data from Sep. 25th (DOY 269) because the measurement and the model have the best agreement on that day. The results are plotted in Fig. 12(b) both in dB and linear form. It is seen from the figure that the number of pods per plant has an approximate linear relationship to the linear $\Delta\sigma^0_{HH-VV}$. Therefore, the number of the pods per plant can be estimated by a least-squares fitting technique to a straight line based on the linear values of $\Delta\sigma^0_{HH-VV}$. In this study, since each pod is assumed to have three beans and there are 13 plants/m^2, the total number of beans/m^2 is 39 times the number of pods per plant. Finally, the number of beans/ m^2 is given as a function of $\Delta\sigma^0_{HH\text{-}VV}$:

$$N = a \cdot \Delta\sigma^0_{HH\text{-}VV} + b \qquad (10)$$

where a = 30165 and b = 671. Note that this approximation can only be applied to the cases in the range 24-40 pods/plant which is a common range for soybean pod counts per plant. In addition, the prediction should not be based on day on which it rains.

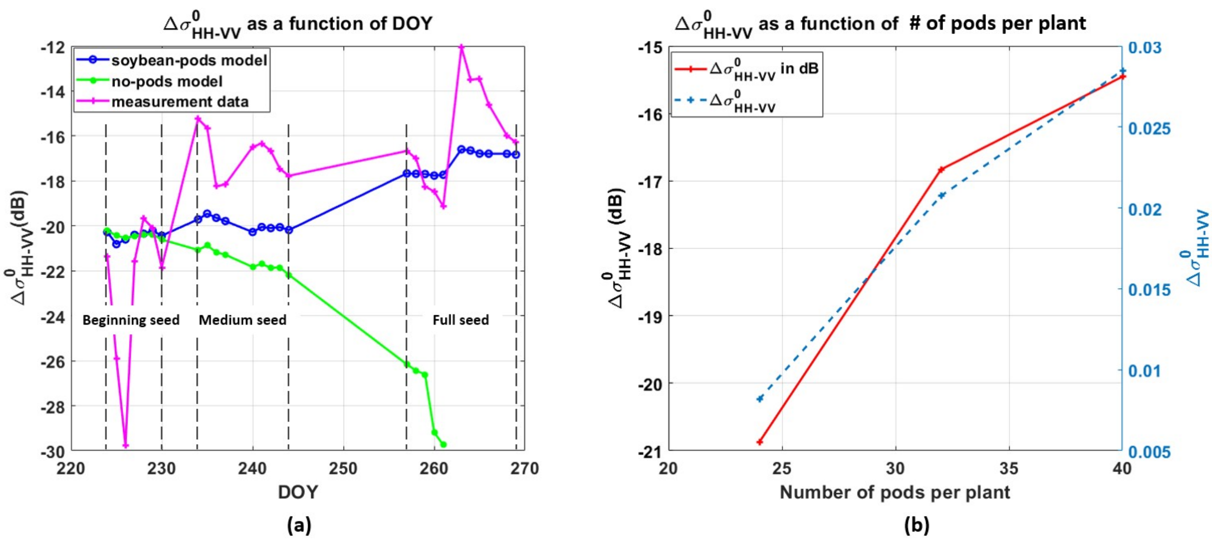

Fig. 12. Relationship between soybean pods and $\Delta\sigma^0_{HH\text{-}VV}$ - (a): $\Delta\sigma^0_{HH\text{-}VV}$ in dB as a function of DOY; (b): $\Delta\sigma^0_{HH\text{-}VV}$ as a function of number of pods per plant.

5. Conclusion

This paper introduces a methodology for analyzing the polarimetric radar backscatter from a soybean field at L-band. A soybean backscattering model is developed by a combined numerical and analytical method to validate the radar experimental data and analyze the contribution of soybean constituents to the backscatter. The numerical method simulates the clustered structure of soybean pods along a vertical stem, while the analytical method treats soybean leaves as thin elliptical discs. Temporal *in situ* data are used in the model to interpret the vegetation dynamics of the soybean field over the growing season.

It is found that the accuracy of the soybean backscatter model is significantly improved when the pods are taken into account. For the model with pods, the RMSEs between the radar data and modeled results are 0.51 dB for VV-pol and 1.1 dB for HH-pol. If the pods are removed from the model, the RMSEs are increased to 1.8 dB for VV-pol and 4.1 dB for HH-pol. Both measured data and modeled results show that the growth of soybean pods results in an increase in the difference between the HH-pol and the VV-pol backscattering ($\Delta\sigma^0_{HH-VV}$). An estimation model is developed to predict the number of beans per square meter from $\Delta\sigma^0_{HH-VV}$ for the full-seed (R6) stage.

The research reported in this paper shows that scientists can not only use L-band radar to monitor the soil moisture, but also to detect the growth of soybean pods. In the future, more field measurements for soybean pods, such as the orientations of pods, can be used to improve the accuracy of the soybean backscattering model. Similar methodology can be applied to other types of crops to further investigate the possibility of using low microwave frequency to detect crop growth and development. Most importantly, extension of these results to larger scales are highly desirable as this can lead to global or regional biophysical parameter retrieval and monitoring.

Acknowledgments

This work was supported by the National Aeronautics and Space Administration (NASA) [grant number: CCLS20896F].

References

Abendroth, L.J., Elmore, R.W., Boyer, M.J., Marlay, S.K., 2011. Corn growth and development. In: Technical Report PMR 1009. Iowa State University Extension, Ames, IA.

Balenzano, A., Mattia, F., Satalino, G., Davidson, M.W.J., 2011. Dense Temporal Series of C- and L- band SAR Data for Soil Moisture Retrieval Over Agricultural Crops. IEEE J. Sel. Top. Appl. Earth Obs. Remote Sens. 4, 439-450, https://doi.org/10.1109/JSTARS.2010.2052916

Casteel, S., 2011. Soybean Physiology: How well do you know soybeans? Purdue University Extension. https://www.agry.purdue.edu/ext/soybean/arrivals/10soydevt.pdf

Chauhan, N.S., Lang, R.H., Ranson, K.J., 1991. Radar modeling of a boreal forest. IEEE Trans. Geosci. Remote Sens. 29, 627-638. https://doi.org/10.1109/36.135825

Chauhan, N.S., Le Vine, D.M., Lang, R.H., 1994. Discrete scatter model for microwave radar and radiometer response to corn: comparison of theory and data. IEEE Trans. Geosci. Remote Sens. 32, 416-426. https://doi.org/10.1109/36.295056

De Roo, R.D., Du, Y., Ulaby, F.T., Dobson, M.C., 2001. A Semi-Empirical Backscattering Model at L-Band and C-Band for a Soybean Canopy with Soil Moisture Inversion. IEEE Trans. Geosci. Remote Sens. 39, 864-872. https://doi.org/10.1109/36.917912

Dobson, M.C., Ulaby, F.T., Hallikainen, M.T., El-Rayes, M.A., 1985. Microwave dielectric behavior of wet soil - Part II: Dielectric mixing models. IEEE Trans. Geosci. Remote Sens. 23, 35-46. https://doi.org/10.1109/TGRS.1985.289498.

Entekhabi, D., Njoku, E. G., O'Neill, P. E., Kellogg, K. H., et al., 2010. The Soil Moisture Active Passive (SMAP) Mission. Proc. IEEE 98, 704-716. https://doi.org/10.1109/JPROC.2010.2043918.

Foldy, L., 1945. The Multiple Scattering of Waves. Phys. Rev. 67, 107-119. https://doi.org/10.1103/PhysRev.67.107

Fung, A.K., Chen, K.S., 2009. Microwave Scatter and Emission Models for Users. Norwood, MA, USA: Artech House

Gregory, A., Clarke, R., 2012. Tables of the complex permittivity of dielectric reference liquids at frequencies up to 5 GHz. NPL Report MAT 23, ISSN 1754-2979

Huang, H., Kim, S., Tsang, L., Xu, X., Liao, T., Jackson, T., Yueh, S., 2015. Coherent Model of L-Band Radar Scattering by Soybean Plants: Model Development, Evaluation, and Retrieval. IEEE J. Sel. Top. Appl. Earth Obs. Remote Sens. 9, 272-284. https://doi.org/10.1109/JSTARS.2015.2469717.

Joerg, H., Pardini, M., Hajnsek, I., Papathanassiou, K. P., 2018. 3-D Scattering Characterization of Agricultural Crops at C-Band Using SAR Tomography. IEEE Trans. Geosci. Remote Sens. 56, 3976 – 3989. https://doi.org/10.1109/TGRS.2018.2818440.

Kankaku, Y., Suzuki, S., Osawa, Y., 2013. ALOS-2 Mission and Development Status. IEEE Geosci. Remote Sens. Symp. Melbourne, Australia. https://doi.org/10.1109/IGARSS.2013.6723302.

Lang, R.H., Sidhu, J., 1983. Electromagnetic Backscattering from a Layer of Vegetation: A Discrete Approach. IEEE Trans. Geosci. Remote Sens. GE-21, 62-71.

https://doi.org 10.1109/TGRS.1983.350531

Lang, R.H., Utku, C., O'Neill, P.E., Tsegaye, T.D., 2004, Role of Albedo in Sensing Soil Moisture under Vegetation with Passive L-band Algorithms. Proc. IEEE Geosci. Remote Sens. Symp. Anchorage, AK, USA, 340-343. https://doi.org/10.1109/IGARSS.2004.1369031.

Lang, R.H., Seker, S., Zhao, Q., Kurum, M., Ogut,M., O'Neill, P.E., Cosh, M., 2014. L-Band Radar Backscattering from a Mature Corn Canopy: Effect of Cobs. Proc. Nat. Radio Sci. Meeting (USNC/URSI), Boulder, CO, USA. https://doi.org/10.1109/USNC-URSI-NRSM.2014.6928036.

Lang, R.H., Sharma, A., Cosh, M., 2017. Scattering from a layer of vegetation: Enhancement effects, Proc. IEEE Geosci. Remote Sens. Symp, Fort Worth, TX, 1419-1421. https://doi.org/10.1109/IGARSS.2017.8127231

Le Vine, D., Schneider, A., Lang, R.H., Carter, H., 1985. Scattering from thin dielectric disks. IEEE Trans. Antennas Propag. 33, 1410-1413. https://doi.org/10.1109/TAP.1985.1143534.

Monsivais-Huertero, A., Judge, J., 2011. Comparison of Backscattering Models at L-Band for Growing Corn. IEEE Geosci. and Remote Sens. Letters 8, 24-28. https://doi.org/10.1109/LGRS.2010.2050459.

O'Neill, P. E., Lang, R. H., Kurum, M., Utku C., Carver, K.R., 2006, Multi-Sensor Microwave Soil Moisture Remote Sensing: NASA's Combined Radar/Radiometer (ComRAD) System. Proc. IEEE MicroRad, SanJuan, 50-54. https://doi.org/10.1109/MICRAD.2006.1677061.

Pedersen, P., 2004. Soybean growth and development. Iowa State University Extension Publications PM1945. https://crops.extension.iastate.edu/files/page/files/SoybeanGrowthandDevelopment.pdf

Peplinski, N.A., Ulaby, F.T., Dobson, M.C., 1995a. Dielectric properties of soils in the 0.3–1.3 GHz range. IEEE Trans. Geosci. Remote Sens. 33, 803–807. https://doi.org/10.1109/36.387598.

Peplinski, N.A., Ulaby, F.T., Dobson, M.C., 1995b. Correction to 'Dielectric properties of soils in the 0.3–1.3 GHz range'. IEEE Trans. Geosci. Remote Sens. 33, 1340. https://doi.org/ 10.1109/ TGRS.1995.477193.

Rosen, P.A., Hensley, S., Shaffer, S., Veilleux, L., Raju Sagi, V., Satish, R., 2015. The NASA-ISRO SAR Mission – An International Space Partnership for Science and Societal Benefit, Proc. IEEE Int. Radar Conference, VA, USA, https://doi.org/ 10.1109/RADAR.2015.7131255.

Rosenqvist, A., Shimada, M., Ito, N., Watanabe, M., 2007. ALOS PALSAR: A Pathfinder Mission for Global-Scale Monitoring of the Environment, IEEE Trans. Geosci. Remote Sens. 45, 3307-3316. https://doi.org/10.1109/TGRS.2007.901027.

Seker, S. S., Schneider, A., 1988. Electromagnetic scattering from a dielectric cylinder of finite length, IEEE Trans. Antennas Propag. 36, 2, 303-307. https://doi.org/10.1109/8.1109.

Sharma, A., Lang, R.H., Kurum, M., O'Neill, P. E., Cosh, M. 2020. L-Band Radar Experiment and Modeling of a Corn Canopy Over a Full Growing Season. IEEE Trans. Geosci. Remote Sens. 99, 1-15, https://doi.org/10.1109/TGRS.2020.2971539

Steele-Dunne, S.C., McNairn, H., Monsivais-Huertero, A., Judge, J., Liu, P.W., Papathanassiou, K., 2017. Radar Remote Sensing of Agricultural Canopies: A Review, IEEE J. Sel. Top. Appl. Earth Obs. Remote Sens. 10, 2249-2273. https://doi.org/10.1109/JSTARS.2016.2639043.

Stuchly, M., Stuchly, S., 1980. Coaxial Line Reflection Methods for Measuring Dielectric Properties of Biological Substances at Radio and Microwave Frequencies-A Review, IEEE Tran. Instru. Meas. 29, 176-183. https://doi.org/10.1109/TIM.1980.4314902.

Thirion-Lefevre, L., Chenerie, I., Galy, C., 2004. Application of a coherent model in simulating the backscattering coefficient of a mangrove forest. Waves Random Media 14, 393–414. https://doi.org/10.1088/0959-7174/14/2/010.

Togliatti, K., Hartman, T., Walker, V.A., Arkebauer, T.J., Suyker, A.E., VanLoocke, A., Hornbuckle, B.K., 2019. Satellite L-band Vegetation Optical Depth is directly Proportional to Crop Water in the US Corn Belt, Remote Sens. Environ. 233, 111378. https://doi.org/10.1016/j.rse.2019.111378

Ulaby, F.T., Sarabandi, K., McDonald, K., Whitt, M., Dobson, M.C., 1988. Michigan Microwave Canopy Scattering Model (MIMICS). Int. J. Remote Sens. 11, 1123–1153. https://doi.org/10.1109/IGARSS.1988.570506

Wang, Q., Jie, L., Zhao, S., Zhang, 2015. Gravimetric Vegetation Water Content Estimation for Corn Using L-Band Bi-Angular, Dual-Polarized Brightness Temperatures and Leaf Area Index. Remote Sens. 7, 10543-10561, https://doi.org/10.3390/rs70810543

Appendix A

DOY	plant height	stem size (l×r)	leaf size (l×w×t)	pod size (l×w×t)	stem #/m^2	leaf #/ m^2	stem biomass	leaf biomass	pod biomass	VSM (m^3/m^3)	Radar HH(dB)	Radar VV(dB)
213	39.3	19×0.25	8.2×6.3 ×0.041	-	13	1274.3	217	151	-	0.0805	-16.82	-17.34
215	-	-	-	-	-	-	-	-	-	0.0652	-17.68	-18.32
216	45.7	33×0.31	9.9×7.3 ×0.035	-	13	1654.7	294	209	-	0.0647	-16.78	-17.05
217	-	-	-	-	-	-	-	-	-	0.0627	-17.77	-18.13

218	-	-	-	-	-	-	-	-	-	0.0575	-17.68	-18.22
221	48.7	33×0.28	8.8×6.0 ×0.031	-	13	1963.3	319	232	-	0.0568	-18.04	-18.06
222	-	-	-	-	-	-	-	-	-	0.0509	-17.43	-17.59
224	-	-	-	-	-	-	-	-	-	0.1225	-14.24	-15.19
225	-	-	-	-	-	-	-	-	-	0.1460	-14.40	-14.73
226	-	-	-	-	-	-	-	-	-	0.1052	-15.86	-16.04
227	-	-	-	-	-	-	-	-	-	0.0963	-14.67	-15.66
228	58.3	41×0.37	10×7.0 ×0.039	-	13	3006	977	553	-	0.0853	-14.43	-15.97
229	-	-	-	-	-	-	-	-	-	0.0711	-15.10	-16.75
230	-	-	-	-	-	-	-	-	-	0.0711	-15.55	-16.71
234	-	-	-	-	-	-	-	-	-	0.1470	-11.77	-14.36
235	-	-	-	-	-	-	-	-	-	0.1131	-12.18	-14.78
236	67.3	49×0.29	8.9×5.3 ×0.025	4.5×0.92 ×0.29	13	2454	611	339	496	0.0882	-14.15	-16.31
237	-	-	-	-	-	-	-	-	-	0.0709	-14.31	-16.62
240	-	-	-	-	-	-	-	-	-	0.1427	-12.73	-15.10
241	-	-	-	-	-	-	-	-	-	0.1144	-12.44	-14.72
242	-	-	-	-	-	-	-	-	-	0.0853	-13.01	-15.46
243	69.3	43×0.34	8.1×5.2 ×0.027	5.0×1.0 ×0.47	13	2318	560	417	617	0.0680	-13.82	-16.28
244	-	-	-	-	-	-	-	-	-	0.0605	-14.01	-16.38
248	-	-	-	4.9×0.90 ×0.61	-	-	667	438	892	-	-	-
254	-	-	-	4.3×0.88 ×0.59	-	-	458	384	850	-	-	-
257	60.3	32×0.42	8.2×5.8 ×0.03	-	13	2343	-	-	-	0.0577	-13.31	-16.00
258	-	-	-	-	-	-	-	-	-	0.0539	-13.72	-16.47
259	-	-	-	-	-	-	-	-	-	0.0514	-14.43	-16.76
260	-	-	-	-	-	-	-	-	-	0.0483	-14.32	-16.43
261	-	-	-	-	-	-	-	-	-	0.0463	-14.68	-16.61
263	67.3	50×0.33	9.2×5.7 ×0.023	4.9×0.90 ×0.75	13	1948	458	306	1052	0.1410	-9.94	-14.09
264	-	-	-	-	-	-	-	-	-	0.1054	-10.70	-13.94
265	-	-	-	-	-	-	-	-	-	0.0845	-11.31	-15.38
266	-	-	-	-	-	-	-	-	-	0.0778	-12.22	-15.97
268	-	-	-	-	-	-	-	-	-	0.0682	-13.47	-17.05
269	57.3	54×0.33	7.7×4.6 ×0.018	4.9×0.83 ×0.73	13	1478	480	283	1148	0.0628	-13.22	-16.18

Table A.1 Soybean measurement data. (Dimensional unit: cm, Biomass unit: g/m^2)

List of Figure Captions

Fig. 1. Soybean plant dimensions as a function of DOY/thermal time.

Fig. 2. Soybean pods - (a): soybean pod at the beginning of stage R5; (b): soybean pod of (a) with half the shell removed; (c): soybean pod at stage R6; (d): soybean pod of (c) with half the shell removed.

Fig. 3. Histogram of leaf orientation.

Fig. 4. (a): GVWC of soybean plant constituents; (b): Wet Biomass of soybean plant constituents.

Fig. 5. ComRAD system mounted on a 19-m boom truck.

Fig. 6. Polarimetric radar backscattering data vs. volumetric soil moisture.

Fig. 7. Ray trajectories for the soybean canopy scattering model.

Fig. 8. Scattering model of soybean pods and stems in FEKO - (a): structure of soybean pod model; (b): multiple pod and stem model at beginning-seed stage; (c): multiple pod and stem model at full-seed stage.

Fig. 9. Leaf parameters fitting: (a) Leaf density (#/m^2); (b) Leaf long radius (cm); (c) Leaf short radius (cm); (d) Leaf thickness (mm).

Fig. 10. Measured data vs. modeling results.

Fig. 11. Scatter plot of measured data against modeled results, where the line represents the least square fit of the scattered points. (a) is for HH-pol and (b) is for VV-pol.

Fig. 12. Relationship between soybean pods and $\Delta\sigma^0_{HH-VV}$: (a) $\Delta\sigma^0_{HH-VV}$ in dB as a function of DOY; (b) $\Delta\sigma^0_{HH-VV}$ as a function of number of pods per plant